NeuroImage 226 (2021) 117559

Contents lists available at ScienceDirect

NeuroImage

journal homepage: www.elsevier.com/locate/neuroimage

Callosal anisotropy predicts attentional network changes after parietal inhibitory stimulation

Selene Schintu[a,b,*], Catherine A. Cunningham[a], Michael Freedberg[a], Paul Taylor[c], Stephen J. Gotts[c], Sarah Shomstein[b], Eric M. Wassermann[a]

[a] National Institute of Neurological Disorders and Stroke, Bethesda, USA
[b] Department of Psychology, George Washington University, Washington DC, USA
[c] National Institute of Mental Health, Bethesda, USA

ARTICLE INFO

Keywords:
fMRI
TMS
DTI
Parietal cortex
Visuospatial attention
Neglect
Resting state functional connectivity

ABSTRACT

Hemispatial neglect is thought to result from disruption of interhemispheric equilibrium. Right hemisphere lesions deactivate the right frontoparietal network and hyperactivate the left via release from interhemispheric inhibition. Support for this putative mechanism comes from neuropsychological evidence as well as transcranial magnetic stimulation (TMS) studies in healthy subjects, in whom right posterior parietal cortex (PPC) inhibition causes neglect-like, rightward, visuospatial bias. Concurrent TMS and fMRI after right PPC TMS show task-dependent changes but may fail to identify effects of stimulation in areas not directly activated by the specific task, complicating interpretations. We used resting-state functional connectivity (RSFC) after inhibitory TMS over the right PPC to examine changes in the networks underlying visuospatial attention and used diffusion-weighted imaging to measure the structural properties of relevant white matter pathways.

In a crossover experiment in healthy individuals, we delivered continuous theta burst TMS to the right PPC and vertex as control condition. We hypothesized that PPC inhibitory stimulation would result in a rightward visuospatial bias, decrease frontoparietal RSFC, and increase the PPC RSFC with the attentional network in the left hemisphere. We also expected that individual differences in fractional anisotropy (FA) of the frontoparietal network and the callosal pathway between the PPCs would account for variability of the TMS-induced RSFC changes.

As hypothesized, TMS over the right PPC caused a rightward shift in line bisection judgment and increased RSFC between the right PPC and the left superior temporal gyrus. This effect was inversely related to FA in the posterior corpus callosum. Local inhibition of the right PPC reshapes connectivity in the attentional network and depends significantly on interhemispheric connections.

1. Introduction

The parietal cortex is a central node of the attentional network (Behrmann et al., 2004). Its crucial role is supported by the literature on neglect patients, in whom a lesion of the right parietal cortex produces loss of awareness of the contralesional side of space (Critchley, 1953; Vallar, 1998; Mort et al., 2003).

According to the interhemispheric competition model anticipated by Sprague in 1966 and a decade later translated into humans by Kinsbourne (Valero-Cabré et al., 2020), hemispatial neglect results from breakdown of the interhemispheric balance normally maintained by reciprocal interhemispheric inhibition (Kinsbourne, 1977). Right parietal lesions causing neglect reduce local function and increase the activity of the contralateral homologous area by releasing it from inhibition, and there is a "push-pull" pattern of right-side re-activation and left-side de-activation in the posterior parietal cortex (PPC) during spontaneous recovery from neglect (Corbetta et al., 2005). Additional support for the interhemispheric competition model comes from transcranial magnetic stimulation (TMS) studies. Nominally inhibitory TMS applied over the left PPC reduces neglect symptomes (for review see Cazzoli et al., 2010), but when it is applied to the right PPC in healthy individuals it causes a temporary, neglect-like, rightward visuospatial bias (Fierro et al., 2000; Hilgetag et al., 2001; Bjoertomt et al., 2002; Hung et al., 2005; Dambeck et al., 2006; Sack et al., 2007; Nyffeler et al., 2008; Cazzoli et al., 2009).

* Corresponding author at: Behavioral Neurology Unit, National Institute of Neurological Disorders and Stroke, Building 10, Room 7D48, 10 Center Drive, MSC 1440, Bethesda, MD 20892-1430, USA
E-mail address: selene.schintu@gmail.com (S. Schintu).

https://doi.org/10.1016/j.neuroimage.2020.117559
Received 29 June 2020; Received in revised form 28 October 2020; Accepted 8 November 2020
Available online 13 November 2020

The role of intrahemispheric connections in visuospatial attention has also been recently highlighted (Bartolomeo et al., 2007a; Lunven et al., 2015; Cazzoli and Chechlacz, 2017). Koch et al. (2008) found that the connection from the left PPC to the ipsilateral primary motor area (M1) is hyperexcitable in neglect patients by delivering conditioning stimulation to the PPC and testing the motor evoked potential from the ipsilateral M1 a few milliseconds later. The PPC-M1 connection is part of the frontoparietal network, which subserves visuospatial attention by connecting the PPC to ipsilateral frontal areas (Doricchi and Tomaiuolo, 2003; Bartolomeo et al., 2007b; He et al., 2007; Thiebaut de Schotten et al., 2011) and excitability in the PPC-M1 pathway is considered a proxy for the state of the network in general. Although the motor evoked potential (MEP) is well understood and easily quantified, it is generated by the corticospinal motor output system whose relationship with the frontoparietal network is not understood. The only direct evidence for the ability of PPC TMS to modulate the functional connectivity of the frontoparietal network consists of a single patient study (Bonnì et al., 2013).

Concurrent TMS/fMRI paradigms measuring task-dependent activation after right PPC inhibitory TMS have found decreased activity in ipsilateral nodes of the frontoparietal network (Sack et al., 2007; Ricci et al., 2012) and increased activation in contralateral regions, such as the primary visual area (Heinen et al., 2011). Using fMRI, Sack et al. (2007) found that the stimulated area was functionally connected to the frontoparietal network bilaterally, but only during task execution. However, task-related activation may fail to identify areas whose connectivity is affected by the stimulation but are not activated by the specific task. Studies of resting-state functional connectivity (RSFC) after PPC TMS can overcome this limitation and provide information on the network independent of its activation.

We used RSFC to study the network effects of nominally inhibitory right PPC TMS in healthy participants. Based on the evidence reviewed above, we hypothesized that inhibition of the right PPC would result in a rightward visuospatial bias with a corresponding decrease in connectivity with ipsilateral frontal areas and/or an increase in connectivity with contralateral areas of the attentional network, due to the release of interhemispheric inhibition.

Diffusion-weighted imaging (DWI) measurement of white matter organization in the frontoparietal network partially accounts for variability in the effect of TMS on attention in healthy individuals (Cazzoli and Chechlacz, 2017). Similarly, DWI of the posterior corpus callosum, which contains the fibers connecting the PPCs (Koch et al., 2011), explains part of the interindividual variability in the attentional shift produced by TMS in healthy individuals (Chechlacz et al., 2015) and influences neglect recovery in patients (Nyffeler et al., 2019). We analyzed DWI using diffusion tensor imaging (DTI) modeling to investigate pathways associated with corresponding changes in RSFC after PPC TMS. We expected that effects on intrahemispheric RSFC would depend on frontoparietal anatomical connectivity, whereas any change in interhemispheric connectivity would depend on the callosal connection between the two PPCs.

2. Materials and methods

2.1. Participants

Seventeen adults (11 women; age = 25.94 ± 1.01 SEM), free of neurological disorders or medications affecting brain function, participated in the study. All had normal or corrected-to-normal vision, were right-handed (Edinburgh Inventory; Oldfield, 1971), and were right-eye dominant (hole-in-card test; Miles, 1930). Participants were compensated and gave written informed consent. The study was approved by the National Institutes of Health, Central Nervous System Institutional Review Board, and conducted in accordance with the ethical standards of the 1964 Declaration of Helsinki (World Medical Association, 2013).

2.2. Procedure

The crossover-design experiment consisted of two separate sessions with a washout period of at least five days. Each session consisted of behavioral testing and fMRI, before and after TMS delivered to the right PPC or the vertex (Fig. 1) in a counterbalanced manner. In each session, participants underwent resting state and anatomical scans. Following the first resting state scan, participants carried out the perceptual and manual line bisection tasks and two tasks assessing spatial bias in proprioceptive (straight-ahead) and sensorimotor (open-loop) pointing performance (Fig. 1). Participants then received TMS over either the right PPC or vertex. Immediately after TMS, participants performed the straight-ahead and open-loop pointing tasks (early post-adaptation), underwent a second resting state scan, and performed the line bisection and pointing tasks again (late post-adaptation). DWI was acquired in a separate session (Fig. 1).

During the tasks, participants were seated in front of a horizontal board with their heads supported by a chinrest. On the board, a target (8 mm in diameter) was positioned at 0 degrees from the body midline, approximately 57cm from participant's nasion and used for open-loop and straight-ahead pointing tasks.

2.3. Behavioral assessment

We used the four tasks described previously in our RSFC study of prism adaptation Schintu et al., (2020b). Here perceptual line bisection was the main outcome measure and the other three were treated as exploratory. We included the exploratory measures to investigate whether inhibition of the right PPC would produce not only the known visuospatial bias (e.g., Fierro et al., 2000; Brighina et al., 2002; Szczepanski and Kastner, 2013), but also proprioceptive and sensorimotor biases as seen following prism adaptation, another intervention modulating visuospatial attention (e.g., Colent et al., 2000; Schintu et al., 2014, 2017).

Perceptual line bisection prioritizes the perceptual, and minimizes the motor, component of visuospatial bias by asking participants to judge a series of pre-bisected lines instead of actively bisecting them. We used a modified version of the Landmark task (Milner et al., 1992). The task consisted of 66 white, pre-bisected, lines (350 mm x ~2 mm) displayed on a black screen positioned 35 cm from the eyes. Lines were transected at the true center and at 2, 4, 6, 8, and 10 mm to the left and right of the true center. Each of the 11 different pre-bisected lines was presented six times in a pseudorandom order, yielding a total of 66 trials, which took approximately three minutes to complete. Each line was displayed for a maximum of five seconds, or until a response was made and was then replaced by a black-and-white patterned mask, which stayed on the screen for one second before the next line was displayed. We used Presentation software (Neurobehavioral Systems, Inc., Berkeley, USA) to generate the stimuli, record responses, and control the task. Participants were instructed to inspect each line and judge whether the transecting mark was closer to the left or right end and to respond within 5 seconds by pressing pedals positioned under the left and right feet. Participants performed at least ten practice trials before the baseline measurement. For each participant, we plotted the percentage of right-side responses as a function of the position of the transector (true center and 2,4,6,8,10 mm to left and right of the true center). We then fit a sigmoid function to the data. The value on the x-axis corresponding to the point at which the participant responded with the right pedal 50% of the time was taken as the point of subjective equality (PSE).

Manual line bisection emphasizes the motor over the perceptual component of the visuospatial bias Milner et al., (1992). We used this task Schenkenberg et al., (1980) to measure the visuospatial shift induced by TMS. It consisted of a series of 10 black lines (identical in size to those used for the perceptual line bisection task) drawn on 297mm x 420mm sheets of paper, which were positioned over the computer screen used for the perceptual line bisection task. Participants were instructed to inspect each line and draw a vertical mark at the perceived

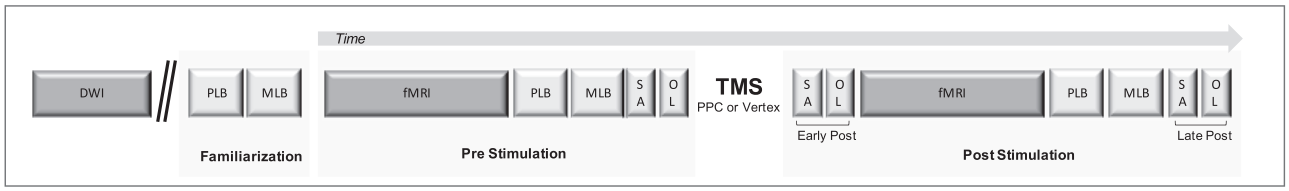

Fig. 1. Experimental timeline of a single session. DWI = diffusion weighted imaging; PLB = perceptual line bisection; MLB = manual line bisection; SA = straight-ahead pointing; OL = open-loop pointing; fMRI = functional magnetic resonance imaging; TMS = transcranial magnetic stimulation.

center of each line with a pen held in the right hand. No time limit was imposed and participants took an average of 1 second to place the mark on one line. We measured the distance between the mark placed by the participant and the true center of the line and took the average as the PSE. Marks to the right of center were coded as positive.

Straight-ahead pointing was used to measure the proprioceptive shift induced by TMS. Participants performed six pointing movements to the midline with the right index finger at a comfortable and uniform speed, while resting their left hands on their laps. Before each movement, participants were told to close their eyes, imagine a line splitting their body in half, and project it onto the board in front of them. We then asked them to point to the projected midline with their eyes closed and then return the hand to the starting position when prompted by the experimenter. To ensure that participants had no visual feedback, the arm and hand were occluded by a cardboard baffle before movement onset. The proprioceptive shift was measured as the average distance between the landing position and the true midline with precision of +/- 0.5 cm.

Open-loop pointing was used to measure the sensorimotor shift induced by TMS. Participants performed six pointing movements with the right index finger to the central (0°) target at a comfortable and uniform speed, while resting their left hands on their laps. Before each movement, we instructed participants to look at the central target, close their eyes, point to the target while keeping their eyes closed, and then return the hand to the starting position when prompted by the experimenter. As in the straight-ahead task, vision of the arm and hand was occluded. The sensorimotor shift was measured as the average distance between the landing position and the central target with a precision of +/- 0.5 cm.

2.4. MRI

2.4.1. MRI acquisition

Functional and structural MRI data were acquired with a 32-channel head coil in 3 Tesla GE medical systems discovery MR750 scanner. Head movement was minimized with padding. A whole-brain T1-weighted anatomical image (MPRAGE) was obtained for each participant (172 slices, voxel size $1.0 \times 1.0 \times 1.0$ mm^3, repetition time (TR) = 7.66 ms, echo time (TE) = 3.476 ms, inversion time (TI) = 1100 ms, field of view (FOV) =$256 \times 156 \times 176$ mm^3, flip angle = 7°). T2* blood oxygen level-dependent (BOLD) resting state scans were acquired for all participants (45 slices aligned to the AC-PC axis, voxel size $3.0 \times 3.0 \times 3.0$ mm^3, TR = 2500 ms, TE = 30.0 ms, FOV = $216 \times 135 \times 216$ mm^3, flip angle 70°, $72 \times 45 \times 72$ acquisition matrix). During resting state scans, lighting was dimmed and participants were instructed to lie still, look at a white central cross appearing on a black screen and, think about nothing.

DWI scans were performed using a 32-channel head coil in a 3 Tesla Siemens Magnetom Prisma scanner. Head movement was minimized with padding. Data were acquired using an echo-planer imaging (EPI) sequence with a voxel size of $2 \times 2 \times 2$ mm^3 and the following parameters: TR = 9200 ms, TE = 79 ms, and matrix size = $110 \times 110 \times 80$. Diffusion imaging was performed in multiple shells, with 70 total diffusion-weighted volumes (10 x b=300 s/mm^2, 60 x b=1100 s/mm^2) and 10 non-diffusion-weighted volumes (b=0 s/mm^2). Two sets of images, with opposite phase-encoded directions (anterior-posterior), were acquired to correct for susceptibility-induced distortion. As anatomical references, high resolution T2-weighted fat-saturated images were acquired with the following parameters: voxel size = $1.1 \times 1.1 \times 1.7$ mm^3, matrix size = $192 \times 192 \times 94$.

2.4.2. MRI preprocessing

We preprocessed the functional and structural MRI data with the AFNI software package (v. 18.2.15; Cox, 1996) and followed the general approach of Schintu et al. (2020b). The anatomical scans were segmented into tissue compartments using the FreeSurfer image analysis suite (Fischl et al., 2002; http://surfer.nmr.mgh.harvard.edu/). We removed the two initial volumes from each resting state scan to allow the magnetic field to stabilize. Volumes were then despiked to minimize outlying time points in each voxel and slice-time corrected to the first slice. Subsequent to this, co-registration of individual EPI volumes to each other and to the anatomical scan and transformation to standard space (Talairach and Tournoux, 1988) at a 2-mm isotropic resolution was accomplished in a single step so that the data were re-gridded only once. Data were then smoothed with an isometric 4-mm full-width half-maximum Gaussian kernel, and we then scaled each voxel time series to a mean of 100, with a range of 0-200. AFNI's 3dTproject was then used to simultaneously censor TRs with head movements > 0.3 mm, bandpass filter the times series between 0.01 and 0.1 Hz and regress the 6 head motion parameters and their first derivatives (Lindquist et al., 2019). Measures of mean framewise displacement were also calculated for use as nuisance covariates in group-level analyses to control for residual global artifacts in the resting-state scans using the AFNI function @1dDiffMag and average voxelwise signal amplitude (standard deviation)(Gotts et al., 2020).

DWI processing was performed using a combination of AFNI's FATCAT programs (Taylor and Saad, 2013) and the TORTOISE software package (v. 3.1.1). Using FATCAT, the T2-weighted anatomical volumes were axialized (rigidly aligned with reference volumes) to provide standard viewing planes (fat_proc_axialize_anat). Additionally, each set of raw DWIs was visually inspected and any volumes with noticeable dropout or motion artifacts were removed from further processing (@djunct_dwi_selector.tcsh and fat_proc_select_vols). TORTOISE's DIFFPREP was used on each set of DWIs to reduce effects of subject motion and eddy current distortion (default settings and options used). DR_BUDDI was then run to correct for B0 inhomogeneities, resulting in a single set of DWIs aligned to the T2-weighted reference for each subject (default options, with distortion level=medium and final resampling to 1.5 mm isotropic voxels). Nonlinear tensor fitting was performed in AFNI (fat_proc_dwi_to_dt), as well as standard RGB-colorized DEC maps of the tensors (fat_proc_decmap). FreeSurfer results were transformed using linear affine alignment with AFNI to map the parcellations into the final diffusion space (fat_proc_map_to_dti). At each processing step, results were checked visually using quality control (QC) images that were automatically generated for each of the above AFNI commands as well as for the TORTOISE commands.

2.4.3. Analysis

2.4.3.1. RSFC. To initiate the analysis, we created a seed region for each participant, composed of a 3mm radius sphere around the coordinates of the stimulation target in the PPC (Fig. 2). The seed voxel time series were first averaged and then correlated (Pearson) with the time

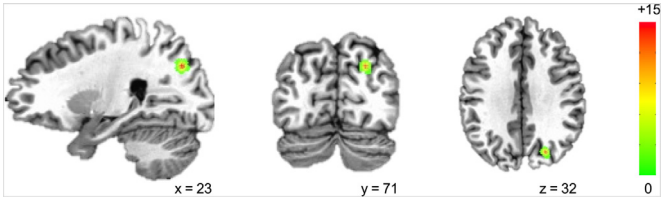

Fig. 2. Overlap of the 17 participants' PPC TMS targets. Color scale indicates number of participants.

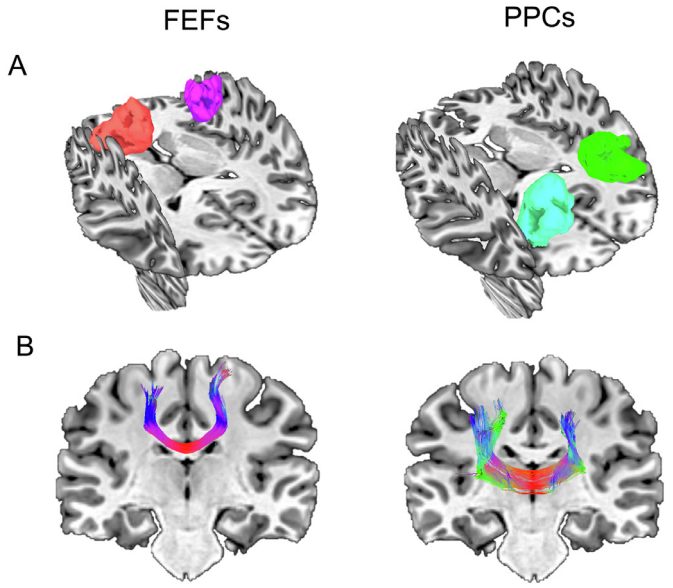

Fig. 3. A. ROIs used to reconstruct transcallosal tracts between left and right IPS1/2 and FEFs. **B.** Reconstructed tracts between the right and left IPS1/2 and FEF, using full probabilistic tractography in 3dTrackID.

series in each voxel throughout the brain, with the correlations transformed by Fisher's z to improve normality. After fMRI preprocessing, we created a mask for each participant including voxels with functional data. For the group analyses, we created a group-level brain mask using voxels where at least 90% of participants had data.

2.4.3.2. DTI. To identify region of interests (ROIs) for the right and left PPC and frontal eye field (FEF), the principal frontal node of the dorsal attentional network (Corbetta and Shulman, 2011), we used a probabilistic atlas of the visual areas (Wang et al., 2015). We located ROIs which would ensure stable and consistent tract reconstruction by transforming the individual combined intraparietal sulcus areas 1 and 2 (IPS1/2) and FEF maps into TT_N27 template space, keeping voxels that had ≥ 30% probability of being in IPS1/2 and FEF (Fig. 3A). Minimal inflation was applied to all ROIs, informed by the white matter skeleton, to enable tracking. Transcallosal tracts between the right and left IPS1/2, and FEF were reconstructed using full probabilistic tractography in 3dTrackID (Taylor and Saad, 2013; Fig. 3B).

2.5. TMS

TMS was delivered with a Magstim Rapid stimulator connected to a figure.-of-eight coil with a diameter of 70 mm. Continuous theta-burst stimulation (3-pulse bursts at 50 Hz delivered every 200 ms; Huang et al., 2005) was delivered at 80% of the active motor threshold (AMT; see below). Stimulation lasted 40 sec with a total of 600 pulses. The electromyogram (EMG) was recorded from the left first dorsal interosseous (FDI) muscle. After finding the scalp location where stimulation evoked the largest motor evoked potential (MEP) from the left FDI, we determined the AMT, defined as the minimum stimulus intensity to produce a MEP > 0.25 mv on 10 consecutive trials, during contraction of the left FDI at approximately 10% of maximum voluntary contraction. Effort was kept constant across participants and over time by monitoring the rectified EMG online.

We used the MRI-guided, Brainsight frameless stereotaxic system (Rogue Research Inc., Montreal, Canada) to record the optimal scalp location for activating the FDI and locate the TMS target. To identify the PPC target we used a probabilistic atlas of the visual areas (Wang et al., 2015) and located the right intraparietal sulcus area 1 (IPS1). We created a visual target for aiming the coil by transforming the IPS1 map from the probabilistic atlas into TT_N27 template space, using voxels with ≥ 30% probability of being in IPS1. We projected the mask of this region into the subject space and targeted the cortical part of the mask. We held the coil tangential to the scalp and rotated the junction of the windings perpendicular to the closest gyrus (Fig. 2). For the vertex condition, identical TMS was applied over the vertex with intersection of the windings in the sagittal plane.

2.6. Statistical analysis

The required sample size was estimated using SAS (version 9.4), based on the mean and standard deviation of change in frontoparietal RSFC from a previous study investigating changes in RSFC following motor learning (Albert et al., 2009). Seventeen participants were required to achieve 80% power to reject the null hypothesis at a significance level of 0.05, two-tailed.

Statistical analyses were performed with SPSS (Version 25.0), Matlab (version R2016a) and AFNI (3dLME command; Cox, 1996) with family-wise alpha set at .05. All data are presented following the recommendation of Weissgerber et al., (2015). Effect sizes are reported as Cohen's *d* or partial eta squared. When sphericity was violated, Greenhouse-Geissser corrected values are reported. We used two-tailed paired t-tests for post-hoc comparisons and Bonferroni-correction when appropriate. When we assessed the behavioral effects of TMS, we excluded participants whose performance deviated from the group mean by two or more standard deviations from the analysis of that task.

RSFC data were submitted to a linear mixed effects (LME) regression model using AFNI's 3dLME with seed-based functional connectivity (correlation maps) as the dependent variable, Time (pre, post), and Stimulation Location (PPC, vertex) as fixed effects, Subject as a random effect, and motion (@1dDiffMag) and average voxel-wise standard deviation as nuisance covariates. Cluster size correction $p < 0.001$ k= 53 (acf-version 3dClustSim; Cox et al., 2017).

The final sample sizes submitted to statistical analysis were 15 for the perceptual line bisection task, 16 for the manual line bisection, 15 for the open-loop pointing task, 15 for the straight-head pointing task, 17 for the DTI and 17 for the RSFC.

3. Results

3.1. Behavior

Paired t-tests comparing baseline performance before PPC and vertex TMS, for each of the four tasks, revealed no significant differences (all $t \leq -1.400$ $p \geq .183$), excluding the possibility of baseline differences driving significant effects and interactions.

3.1.1. Perceptual line bisection

A repeated measures ANOVA, with Time (pre, post) and Stimulation Location (PPC, vertex) as within-participants variables, revealed a significant Time by Stimulation Location interaction [$F(1, 14) = 6.084$, $p = 0.027$, η^2_p=0.303; Fig. 4]. Post-hoc comparison showed that when TMS was delivered over the PPC the PSE shifted significantly rightward from pre (-0.73 mm) to post [-0.07 mm; $t(14) = -2.171$, $p = 0.048$, Cohen's $d = 0.560$], but not when TMS was delivered over the vertex

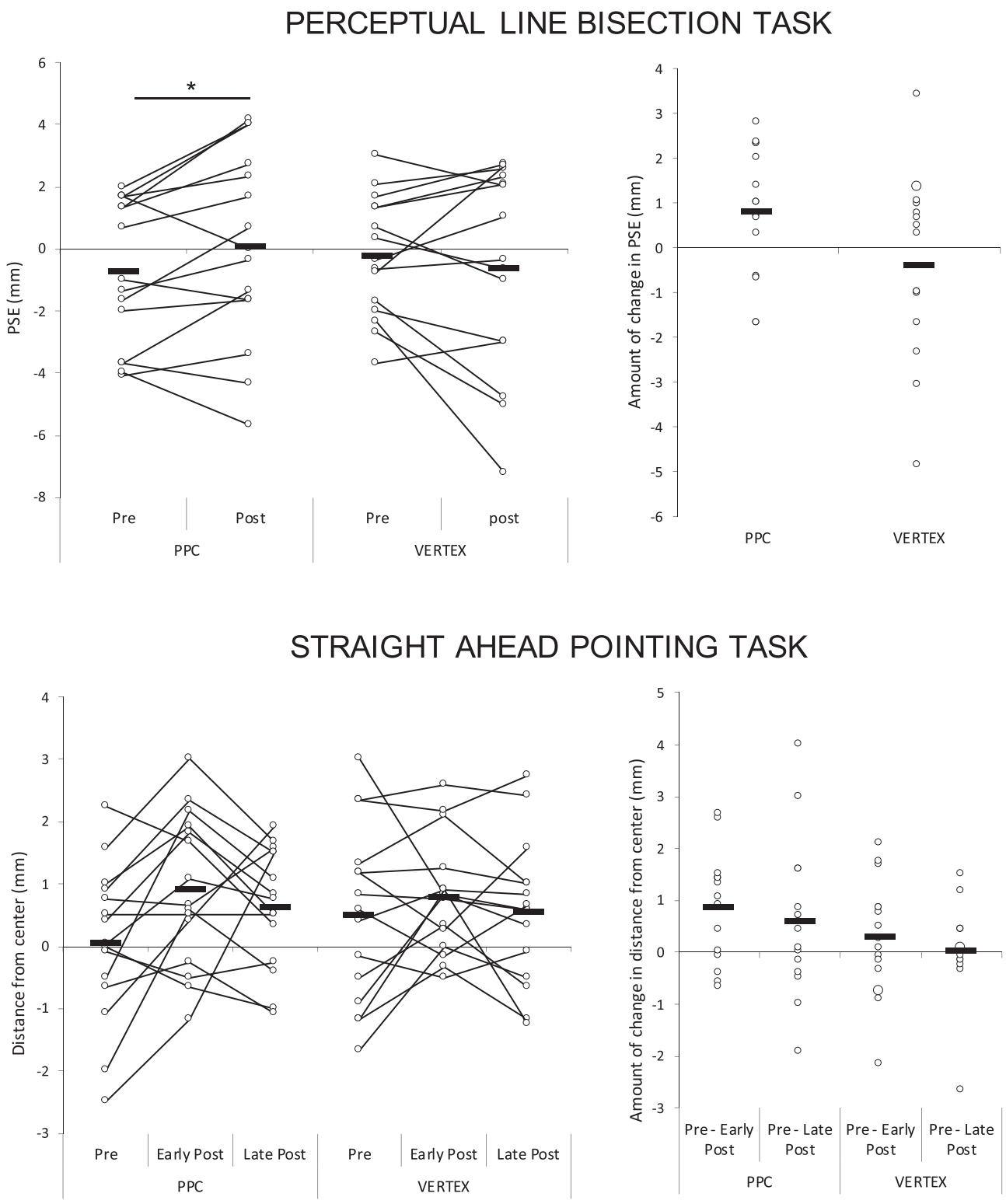

Fig. 4. Effects of TMS on perceptual line bisection and straight-ahead pointing tasks. Negative and positive values represent left and right of center, respectively. Bold horizontal lines represent group means. * $p < 0.05$.

[t(14) = 0.739, p = 0.472, Cohen's d = 0.190]. All other effects were non-significant (all F ≤ 0.299, p ≥ .593).

3.1.2. Manual line bisection

Repeated measures ANOVA, with Time (pre, post) and Stimulation Location (PPC, vertex) as within-participants variables, showed no significant main effect or interaction (all F ≤ .507, p ≥ .487).

3.1.3. Straight-ahead pointing

We measured proprioceptive performance by quantifying the deviation in the pointing between the participants' perceived and true midline. Repeated measures ANOVA, with Time (pre, early-post, late-post) and Stimulation Location (PPC, vertex) as within-participant variables, revealed a significant main effect of Time [F(2, 28) = 4.687, p = 0.018, η^2_p = 0.251; Fig. 4]. Post-hoc comparison revealed that, inde-

pendently of the Stimulation Location, the pointing error shifted significantly rightward from pre (0.27 cm) to early-post [0.85 cm; t (14) = -2.993, p = 0.020 Bonferroni corrected, Cohen's d = 0.772], but not to late-post [0.58 cm; t (14) = -1.458, p = .334 Bonferroni corrected, Cohen's d = 0.376]. All other effects where non-significant (all $F \leq 1.090$, $p \geq .350$).

3.1.4. Open-loop pointing

We measured sensorimotor performance by quantifying the deviation between the landing position and the true center. Repeated measures ANOVA, with Time (pre, early-post, late-post) and Stimulation Location (PPC, vertex) as within-participant variables, revealed no significant main effect or interaction (all $F \leq 3.717$, $p \geq .074$).

3.2. RSFC

3.2.1. Seed-based analyses

Before covarying head motion and the average standard deviation nuisance measures in the LME, we checked for significant baseline differences in the nuisance variables between the PPC and vertex stimulation sessions with a series of two-tailed paired t-tests. We found no differences at baseline [motion t(16) = 1.301, p = .212; standard deviation t(16) = .211, p = .835; PPC: motion mean = .064 (SEM = .006), standard deviation = 1.149 (0.048); vertex motion = .056 (.006), standard deviation = 1.137 (0.054))], or at post [(motion t(16) = -.219, p = .829; standard deviation t(16) = -.949, p = .357; PPC: motion = .071 (.010), standard deviation = 1.162 (.068); vertex: motion .073 (.008), standard deviation = 1.229 (.058)]. Similarly, there was no significant difference between the pre- and post- phases for both the PPC [motion t(16) = .953, p = .355 deviation t(16) = .297, p = .770] and vertex [motion t(16) = 2.040, p = .058; standard deviation t(16) = 1.483, p = .172].

The LME analysis revealed a significant Time x Stimulation Location interaction (p = 0.001, corrected), such that RSFC was differentially affected according to the stimulation site. The analysis detected the left superior temporal gyrus (STG; BA41; 59 voxels = 177 mm^3; x = -37 y = -31 z = 16; LPI coordinate system; Fig. 5A) as a significant cluster relative to the right IPS1 seed.

To follow up the Time x Stimulation Location interaction for each stimulation location, we extracted the time series of the cluster that survived the LME and computed the correlation between the cluster and IPS1 timeseries. We averaged the time series of all voxels in this cluster, and then compared the Fisher z-transformed correlation coefficient before and after TMS. Post-hoc testing of the correlation coefficients revealed that PPC TMS increased RSFC between the right IPS1 and left STG seeds [t(16) = 2.989, p = 0.009 Cohen's d = 0.72; pre = 0.15, post = 0.26], whereas vertex TMS was associated with decreased RSFC between the right IPS1 and left STG [t(16) = -3.331, p = 0.004 Cohen's d = 0.80; pre = 0.28, post = 0.14] (Fig. 5B).

To rule out the possibility that our results were driven by baseline differences between the two stimulation conditions, we performed a repeated measures ANOVA with the change in RSFC (post - pre) as the independent variable, Stimulation Location as the within participants variable, and baseline RSFC as a covariate. The results still showed a significant main effect of Stimulation Location [F(1, 14) = 9.817 p = 0.007, $\eta^2_p = 0.412$].

Interindividual variance in the change in RSFC between the right IPS1 and left STG was significantly influenced by FA between the two PPCs when TMS was delivered over the right PPC (r = -0.539, p = 0.026; Fig. 6), but not by FA between the FEFs (r = -.279, p = .278). Callosal FA between PPCs and FEFs were strongly correlated within individuals (r = .631, p = .007).

While volume-based analysis in standard space is a common approach in the field, it can introduce uncertainty in the estimate of the location of results at the group level. To assess individual variability, we non-linearly registered the standard space anatomies for each subject with the MNI 2009c asymmetric template and applied the same warp used for each subject to the STG cluster detected in the group analyses. This allowed us to compare each subject-specific aligned cluster to the Brodmann atlas and to their individual anatomies. The group-level STG cluster was centered in the medial portion of Heschl's gyri, which is putative BA41. When examining the peak location of this group-level cluster relative to the individual-subject anatomies that contributed to the result (see Table 1), 11 of 17 were centered in putative BA41, five in the dorsal bank of the lateral sulcus, defined as OP1(e.g., Eickhoff et al., 2006) and thus as putative BA40, and one at the boundary of putative BA40 and BA41. We concluded that, while the STG cluster was centered on Heschl's gyus on average, we cannot rule out some contribution from the adjacent parietal cortex to the results.

Table 1
Report of peak location (MNI 2009c asymmetric template) of the group-level cluster relative to the individual-subject anatomies.

Subject	BA	X	Y	Z
S1	41	-42	-30	14
S2	41	-40	-29	14
S3	41	-45	-27	14
S4	41	-43	-27	16
S5	41	-42	-29	13
S6	41	-42	-30	13
S7	40	-46	-30	13
S8	41	-42	-30	13
S9	41	-45	-26	13
S10	40	-46	-34	15
S11	40	-46	-32	15
S12	40	-44	-30	15
S13	41	-44	-29	15
S14	41	-44	-29	13
S15	40/41	-43	-30	15
S16	41	-45	-30	13
S17	40	-46	-30	15

4. Discussion

We hypothesized that inhibitory TMS delivered to the right PPC of healthy individuals would produce a rightward visuospatial bias, decrease the intrahemispheric RSFC between the stimulated right PPC and frontal areas and increase RSFC with areas of the contralateral hemisphere. We also expected that subtending structural connectivity would predict the magnitude of RSFC changes.

As expected, inhibiotry TMS of the right PPC produced a rightward visuospatial bias, as measured by the perceptual line bisection task. This finding reproduces previously reported results (e.g., Fierro et al., 2000; Szczepanski and Kastner, 2013) and, since the behavioral data were collected at the end of the experiment, shows that the TMS-induced effect was active during the fMRI acquisition. We also found a rightward shift in the perceived midline on the straight-ahead pointing task. However, this shift was only present at the early-post measurement. The direction of change is consistent with inhibition of the right PPC and the trend is visible in Fig. 4. However, it was not borne out by a significant Time x Stimulation Location interaction. The absence of a statistically significant change on this behavioral measure is not surprising, since feedback from the motor performance requirement of the task likely reversed the visuospatial modulation (Schintu et al., 2020a). Unlike Cazzoli and Chechlacz (2017), we found a significant change in the perceptual, but not the manual, line bisection task following right PPC TMS. The reason for this discrepancy may lie in the difference in subjects selection between the two studies. Since their focus was on individual differences, Cazzoli and Chechlacz (2017) did not select participants by handedness. We, by contrast, selected participants based on handedness and eye dominance, which has been shown to interact with visuospatial attention (Schintu et al., 2020a). In a previous sample drawn from the same population of right handed, right-eyed individuals, we found significant

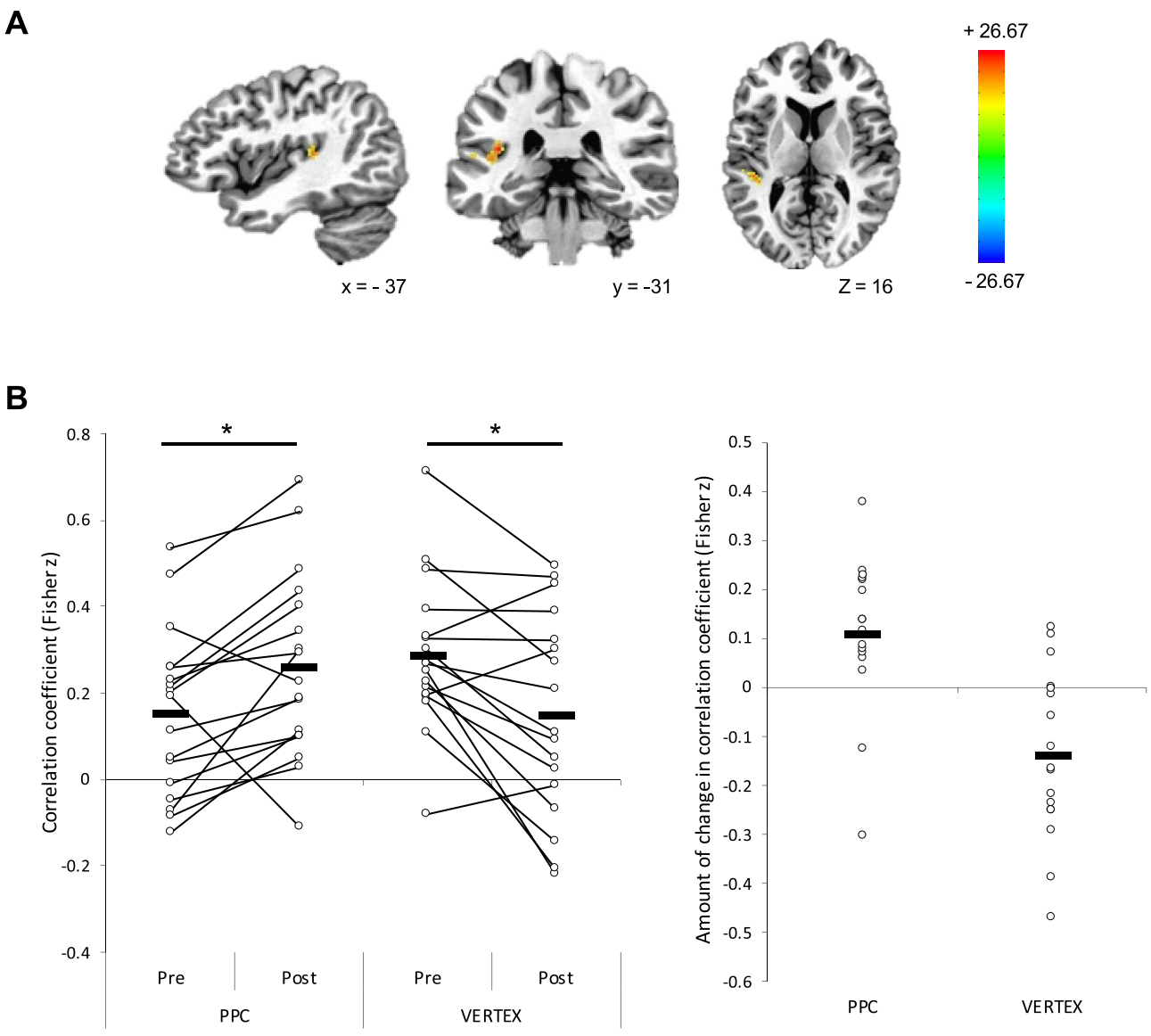

Fig. 5. RSFC seed based analysis. **A.** Significant clusters of RSFC change from the Time x Stimulation Location interaction. Color scale indicates F-value. LPI coordinate system. **B.** RSFC between left STG and the right IPS1/2 seed. **C.** Amount of change (post - pre) in RSFC between the left STG and the IPS1/2 seed. *p < .05. Bold horizonal lines represents group means.

group-level leftward attentional bias on perceptual, but not manual, line bisection (Schintu et al., 2020a). This is not surprising, given that the perceptual line bisection task prioritizes the perceptual, and minimizes the motor, component of attention, and is thus a more sensitive measure of visuospatial bias (Milner et al., 1992).

Seed-based analysis of RSFC at the whole-brain level showed that TMS of the right PPC increased its RSFC with the left STG. The STG has been cited, along with the PPC (Critchley, 1953) and inferior parietal lobule (IPL; Vallar and Perani, 1986; Mort et al., 2003), as the source of hemispatial neglect when lesioned in both monkeys and humans (Karnath et al., 2001). The STG is generally considered part of the ventral attentional network (Shulman et al., 2010), which generates the non-spatial component of attention. However, STG activity also influences the dorsal network, which provides the spatial component (Corbetta and Shulman, 2011). Support for STG involvement in spatial attention comes from neglect patients in whom impaired functional connectivity between STG and middle frontal gyrus (MFG) has been shown to correlate with the impaired interhemispheric parietal connectivity, which is in turn associated with the severity of the attentional deficit (He et al., 2007). STG inhibition by TMS affects allocentric, object-based, spatial processing (Ellison et al., 2004; Shah-Basak et al., 2018). This is also consistent with a lesion study employing the Ota search and a reading task to quantify object-based neglect (Verdon et al., 2010) and with both fMRI (Galati et al., 2000; Neggers et al., 2006) and TMS (Shah-Basak et al., 2018) studies employing versions of the line bisection tasks in healthy individuals. It is noteworthy that the left STG cluster that increased RSFC with the right PPC seed is close to Heschl's gyrus where early cortical auditory processing occurs (Tzourio et al., 1997). This change in RSFC cannot be attributed to the TMS auditory artifact (Siebner et al., 1999), since the connectivity change was unilateral, whereas the auditory artifact is binaural and the direction of change was not identical in the PPC and vertex conditions where the auditory stimulation was comparable.

Despite our aim to investigate the effect of inhibitory TMS over the PPC at the group level, we recognize the importance of idiosyncrasies in functional brain organization (Lynch et al., 2019). The volume-based analysis allows robust whole-brain analyses of both cortex and subcortical brain. However, along with this advantage there is some intrinsic

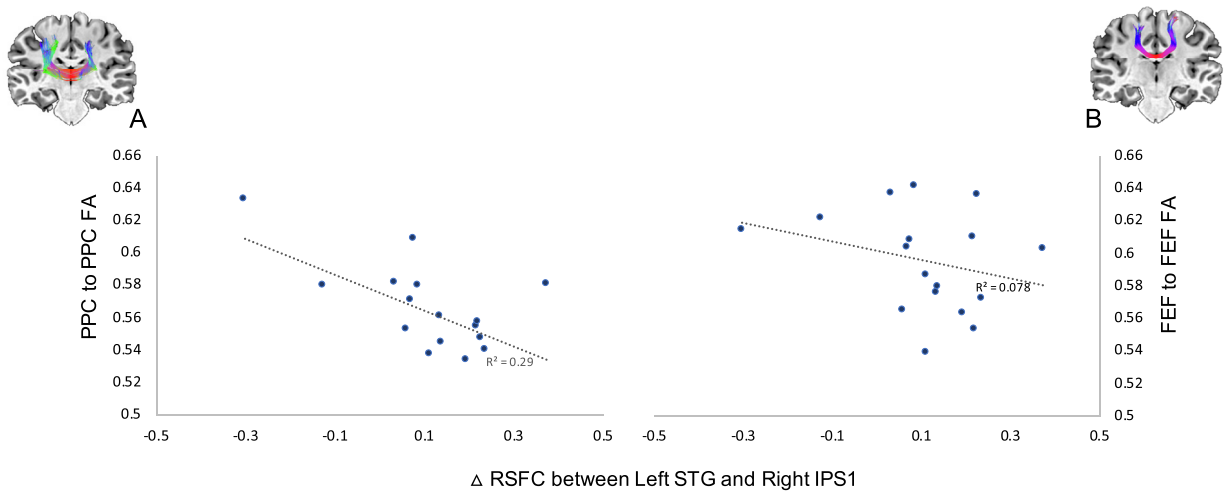

Fig. 6. Association between the amount of change in RSFC between the left STG and right IPS1/2 seed after TMS and callosal FA between **A.** left and right PPC and **B.** FEF, across participants.

uncertainty in estimating the anatomical location of the results. Spatial blurring, which can help reduce the contribution of thermal noise to measured signals and improve spatial overlap across subjects at the group level, can blend adjacent, but functionally distinct, anatomical signals. Individual variation in registration to a standard template can also lead to uncertainty in localization. Therefore, we acknowledge that, because of the fMRI analysis method employed, we cannot exclude the possibility that there was some contribution of the adjacent left PPC (BA40) to the cluster detected in the left STG (BA 41). The possible involvement of left BA 40 would not be surprising since this portion of the PPC is activated during perceptual line bisection tasks (e.g., Fink et al., 2001). Furthermore, since such task-driven activations have been found mainly in the right hemisphere (Ciçek et al., 2009; Cavézian et al., 2012; Seydell-Greenwald et al., 2019), it would support the reshaping of the attentional network following temporary disruption of the right PPC.

As expected, we found a change in interhemispheric RSFC at the group level, but not between homologous regions of the PPC as we predicted based on previous studies. This is surprising if framed by the interhemispheric rivalry theory and the re-activation of the right PPC and de-activation of the left in recovery from neglect (Corbetta et al., 2005). However, a previous study (Ricci et al., 2012) applying TMS over the right PPC in healthy participants found a bilateral decrease in PPC activation, as though the PPCs were affected in parallel. This apparent inconsistency can be explained by task *versus* rest dichotomy. Another instance of the two PPCs behaving similarly comes from a recent study from our laboratory (Schintu et al., 2020b) where we investigated the changes in RSFC after adaptation to left-shifting prisms and found a bilateral decrease in RSFC in both PPCs, along with the expected, neglect-like, leftward, shift in attentional bias previously described (Schintu et al., 2014). The existence of PPC-to-PPC inhibition has been shown in healthy individuals by online TMS effects on behavior (Szczepanski and Kastner, 2013) and TMS-related electrophysiological measures (Koch et al., 2011). Based on these and our earlier results (Schintu et al., 2020b), it seems that rivalry between the PPCs in healthy individuals is present only when one PPC is preferentially activated, either by task engagement or TMS. This also appears to be true for the primary motor areas, which are also linked by inhibitory connections Ferbert et al., (1992). There, unilateral muscle contraction increases inhibitory signaling from the activated motor area to its contralateral homolog (Vercauteren et al., 2008). While fMRI activation and TMS studies have found evidence of reciprocal inhibition between the PPCs, RSFC, which measures temporal correlations between active areas, might not show changes in connectivity if the PPCs are inactive at rest. It is also possible that a change in RSFC between the two PPCs was present in this study but did not survive the cluster threshold.

The reshaping of the attentional network following temporary disruption of the right PPC is further supported by the correlation between PPC-to-PPC white matter FA and the magnitude of RSFC change across participants. As noted in the introduction, structural connectivity of the posterior corpus callosum predicts the interhemispheric effects of PPC TMS (Koch et al., 2011) and acute recovery from neglect Lunven et al., (2015) and it has been proposed that robust posterior callosal connections facilitate compensation for right parietal damage by promoting the integration of the attentional networks across hemispheres (Lunven et al., 2015). Taken together, these findings suggest that the facilitation/inhibition dichotomy may be too simplistic to capture the operation of this network and that interaction of intra- and interhemispheric pathways should be considered more in detail (Bartolomeo, 2019).

The negative correlation between callosal FA and change in RSFC implies that stronger structural connectivity between the two PPCs protects against TMS-induced disruption. It is possible that in participants with more robust callosal pathways, inhibitory TMS of the right PPC was less effective in reversing the intrinsic right-to-left PPC inhibition (Koch et al., 2011) than in those with weaker anatomical connectivity and lower right-to-left PPC inhibition at baseline.

In conclusion, we have shown that inhibition of the right PPC causes reorganization of the attentional network, detectable at rest, and that the change in RSFC is mediated by the callosal connection between the PPCs. These findings also underscore the integral role of the STG in the function of the attentional network, further supporting the involvement of callosal connectivity in the modulation of attention.

5. Data and code availability statement

The data and code that support the findings of this study are available from the corresponding author upon reasonable request in agreement with NIH policy

Credit authorship contribution statement

Selene Schintu: Conceptualization, Investigation, Formal analysis, Writing – original draft, Funding acquisition. **Catherine A. Cunningham:** Investigation, Formal analysis. **Michael Freedberg:** Methodology, Writing – review & editing. **Paul Taylor:** Supervision, Methodol-

ogy. **Stephen J. Gotts:** Supervision, Writing – review & editing. **Sarah Shomstein:** Conceptualization, Writing – review & editing, Funding acquisition. **Eric M. Wassermann:** Conceptualization, Writing – original draft, review & editing, Funding acquisition.

Declaration of Competing Interest

The authors declare no conflict of interest.

Acknowledgments

We would like to thank Drs. Joelle Sarlls and Vinai Roopchansingh for their support in designing MRI sequences.

Funding sources

This work was supported by the National Institutes of Health Ruth L. Kirschstein National Research Service Award to Dr. Schintu, the National Institute of Neurological Disorders and Stroke (1ZIANS002977-20) to Drs. Schintu, Wassermann and Freedberg, the National Science Foundation (grants BCS-1534823 and BCS-1921415) to Prof. Shomstein, the National Institute of Neurological Disorders and Stroke and the National Institute of Mental Health Intramural Research Programs (ZICMH002888) to Dr. Taylor, the Center for Neuroscience and Regenerative Medicine (CNRM-70-3904) to Dr. Freedberg, and the National Institute of Mental Health Intramural Research Programs to Dr. Gotts.

Reference

Albert, NB, Robertson, EM, Miall, RC, 2009. The resting human brain and motor learning. Curr. Biol. 19, 1023–1027.
Bartolomeo, P, 2019. Visual neglect: getting the hemispheres to talk to each other. Brain 142, 840–842.
Bartolomeo, P, Thiebaut de Schotten, M, Doricchi, F, 2007a. Left unilateral neglect as a disconnection syndrome. Cereb. Cortex 17, 2479–2490.
Bartolomeo, P, Thiebaut de Schotten, M, Doricchi, F, 2007b. Left unilateral neglect as a disconnection syndrome. Cereb. Cortex N Y N 1991 17, 2479–2490.
Behrmann, M, Geng, JJ, Shomstein, S, 2004. Parietal cortex and attention. Curr. Opin. Neurobiol. 14, 212–217.
Bjoertomt, O, Cowey, A, Walsh, V, 2002. Spatial neglect in near and far space investigated by repetitive transcranial magnetic stimulation. Brain J. Neurol. 125, 2012–2022.
Bonnì, S, Mastropasqua, C, Bozzali, M, Caltagirone, C, Koch, G, 2013. Theta burst stimulation improves visuo-spatial attention in a patient with traumatic brain injury. Neurol. Sci. 34, 2053–2056.
Brighina, F, Bisiach, E, Piazza, A, Oliveri, M, La Bua, V, Daniele, O, Fierro, B, 2002. Perceptual and response bias in visuospatial neglect due to frontal and parietal repetitive transcranial magnetic stimulation in normal subjects. Neuroreport 13, 2571.
Cavézian, C, Valadao, D, Hurwitz, M, Saoud, M, Danckert, J, 2012. Finding centre: ocular and fMRI investigations of bisection and landmark task performance. Brain Res. 1437, 89–103.
Cazzoli, D, Chechlacz, M, 2017. A matter of hand: causal links between hand dominance, structural organization of fronto-parietal attention networks, and variability in behavioural responses to transcranial magnetic stimulation. Cortex 86, 230–246.
Cazzoli, D, Müri, RM, Hess, CW, Nyffeler, T, 2009. Horizontal and vertical dimensions of visual extinction: a theta burst stimulation study. Neuroscience 164, 1609–1614.
Cazzoli, D, Müri, RM, Hess, CW, Nyffeler, T, 2010. Treatment of hemispatial neglect by means of rTMS–a review. Restor. Neurol. Neurosci. 28, 499–510.
Chechlacz, M, Humphreys, GW, Sotiropoulos, SN, Kennard, C, Cazzoli, D, 2015. Structural organization of the corpus callosum predicts attentional shifts after continuous theta burst stimulation. J. Neurosci. Off J. Soc. Neurosci. 35, 15353–15368.
Ciçek, M, Deouell, LY, Knight, RT, 2009. Brain activity during landmark and line bisection tasks. Front. Hum. Neurosci. 3, 7.
Colent, C, Pisella, L, Bernieri, C, Rode, G, Rossetti, Y, 2000. Cognitive bias induced by visuo-motor adaptation to prisms: a simulation of unilateral neglect in normal individuals? Neuroreport 11.
Corbetta, M, Kincade, MJ, Lewis, C, Snyder, AZ, Sapir, A, 2005. Neural basis and recovery of spatial attention deficits in spatial neglect. Nat. Neurosci. 8, 1603–1610.
Corbetta, M, Shulman, GL, 2011. Spatial neglect and attention networks. Annu. Rev. Neurosci. 34, 569–599.
Cox, RW, 1996. AFNI: software for analysis and visualization of functional magnetic resonance neuroimages. Comput. Biomed. Res. Int. J. 29, 162–173.
Cox, RW, Chen, G, Glen, DR, Reynolds, RC, Taylor, PA, 2017. FMRI clustering in AFNI: false-positive rates redux. Brain Connect. 7, 152–171.
Critchley, M, 1953. The Parietal Lobes. Hafner Press, UK.
Dambeck, N, Sparing, R, Meister, IG, Wienemann, M, Weidemann, J, Topper, R, Boroojerdi, B, 2006. Interhemispheric imbalance during visuospatial attention investigated by unilateral and bilateral TMS over human parietal cortices. Brain Res. 1072, 194–199.
Doricchi, F, Tomaiuolo, F, 2003. The anatomy of neglect without hemianopia: a key role for parietal-frontal disconnection? Neuroreport 14, 2239–2243.
Eickhoff, SB, Schleicher, A, Zilles, K, Amunts, K, 2006. The human parietal operculum. I. cytoarchitectonic mapping of subdivisions. Cereb. Cortex 16, 254–267.
Ellison, A, Schindler, I, Pattison, LL, Milner, AD, 2004. An exploration of the role of the superior temporal gyrus in visual search and spatial perception using TMS. Brain 127, 2307–2315.
Ferbert, A, Priori, A, Rothwell, JC, Day, BL, Colebatch, JG, Marsden, CD, 1992. Interhemispheric inhibition of the human motor cortex. J. Physiol. 453, 525–546.
Fierro, B, Brighina, F, Oliveri, M, Piazza, A, La Bua, V, Buffa, D, Bisiach, E, 2000. Contralateral neglect induced by right posterior parietal rTMS in healthy subjects. Neuroreport 11, 1519–1521.
Fink, GR, Marshall, JC, Weiss, PH, Zilles, K, 2001. The neural basis of vertical and horizontal line bisection judgments: an fMRI study of normal volunteers. Neuroimage 14, S59–S67.
Fischl, B, Salat, DH, Busa, E, Albert, M, Dieterich, M, Haselgrove, C, van der Kouwe, A, Killiany, R, Kennedy, D, Klaveness, S, Montillo, A, Makris, N, Rosen, B, Dale, AM, 2002. Whole brain segmentation: automated labeling of neuroanatomical structures in the human brain. Neuron 33, 341–355.
Galati, G, Lobel, E, Vallar, G, Berthoz, A, Pizzamiglio, L, Le Bihan, D, 2000. The neural basis of egocentric and allocentric coding of space in humans: a functional magnetic resonance study. Exp. Brain Res. 133, 156–164.
Gotts, SJ, Gilmore, AW, Martin, A, 2020. Brain networks, dimensionality, and global signal averaging in resting-state fMRI: Hierarchical network structure results in low-dimensional spatiotemporal dynamics. Neuroimage 205, 116289.
He, BJ, Snyder, AZ, Vincent, JL, Epstein, A, Shulman, GL, Corbetta, M, 2007. Breakdown of functional connectivity in frontoparietal networks underlies behavioral deficits in spatial neglect. Neuron 53, 905–918.
Heinen, K, Ruff, CC, Bjoertomt, O, Schenkluhn, B, Bestmann, S, Blankenburg, F, Driver, J, Chambers, CD, 2011. Concurrent TMS–fMRI reveals dynamic interhemispheric influences of the right parietal cortex during exogenously cued visuospatial attention. Eur. J. Neurosci. 33, 991–1000.
Hilgetag, CC, Théoret, H, Pascual-Leone, A, 2001. Enhanced visual spatial attention ipsilateral to rTMS-inducedvirtual lesions' of human parietal cortex. Nat. Neurosci. 4, 953–958.
Huang, Y-Z, Edwards, MJ, Rounis, E, Bhatia, KP, Rothwell, JC, 2005. Theta burst stimulation of the human motor cortex. Neuron 45, 201–206.
Hung, J, Driver, J, Walsh, V, 2005. Visual selection and posterior parietal cortex: effects of repetitive transcranial magnetic stimulation on partial report analyzed by Bundesen's theory of visual attention. J. Neurosci. Off J. Soc. Neurosci. 25, 9602–9612.
Karnath, H-O, Ferber, S, Himmelbach, M, 2001. Spatial awareness is a function of the temporal not the posterior parietal lobe. Nature 411, 950–953.
Kinsbourne, M, 1977. Hemi-neglect and hemisphere rivalry. Adv. Neurol. 18, 41.
Koch, G, Cercignani, M, Bonnì, S, Giacobbe, V, Bucchi, G, Versace, V, Caltagirone, C, Bozzali, M, 2011. Asymmetry of parietal interhemispheric connections in humans. J. Neurosci. 31, 8967–8975.
Koch, G, Oliveri, M, Cheeran, B, Ruge, D, Lo Gerfo, E, Salerno, S, Torriero, S, Marconi, B, Mori, F, Driver, J, Caltagirone, C, Rothwell, JC, 2008. Hyperexcitability of parietal–motor functional connections in the intact left-hemisphere of patients with neglect. Brain 131, 3147–3155.
Lindquist, NC, de Albuquerque, CDL, Sobral-Filho, RG, Paci, I, Brolo, AG, 2019. High-speed imaging of surface-enhanced Raman scattering fluctuations from individual nanoparticles. Nat. Nanotechnol. 14, 981–987.
Lunven, M, Thiebaut De Schotten, M, Bourlon, C, Duret, C, Migliaccio, R, Rode, G, Bartolomeo, P, 2015. White matter lesional predictors of chronic visual neglect: a longitudinal study. Brain 138, 746–760.
Lynch, CJ, Breeden, AL, Gordon, EM, Cherry, JBC, Turkeltaub, PE, Vaidya, CJ, 2019. Precision inhibitory stimulation of individual-specific cortical hubs disrupts information processing in humans. Cereb. Cortex 29, 3912–3921.
Miles, WR, 1930. Ocular dominance in human adults. J. Gen. Psychol. 3, 412–430.
Milner, AD, Brechmann, M, Pagliarini, L, 1992. To halve and to halve not: an analysis of line bisection judgements in normal subjects. Neuropsychologia 30, 515–526.
Mort, DJ, Malhotra, P, Mannan, SK, Rorden, C, Pambakian, A, Kennard, C, Husain, M, 2003. The anatomy of visual neglect. Brain 126, 1986–1997.
Neggers, SFW, Van der Lubbe, RHJ, Ramsey, NF, Postma, A, 2006. Interactions between ego- and allocentric neuronal representations of space. Neuroimage 31, 320–331.
Nyffeler, T, Cazzoli, D, Wurtz, P, Lüthi, M, von Wartburg, R, Chaves, S, Déruaz, A, Hess, CW, Müri, RM, 2008. Neglect-like visual exploration behaviour after theta burst transcranial magnetic stimulation of the right posterior parietal cortex. Eur. J. Neurosci. 27, 1809–1813.
Nyffeler, T, Vanbellingen, T, Kaufmann, BC, Pflugshaupt, T, Bauer, D, Frey, J, Chechlacz, M, Bohlhalter, S, Müri, RM, Nef, T, Cazzoli, D, 2019. Theta burst stimulation in neglect after stroke: functional outcome and response variability origins. Brain 142, 992–1008.
Oldfield, RC, 1971. The assessment and analysis of handedness: the Edinburgh inventory. Neuropsychologia 9, 97–113.
Ricci, R, Salatino, A, Li, X, Funk, A, Logan, S, Mu, Q, Johnson, K, Bohning, D, George, M, 2012. Imaging the neural mechanisms of TMS neglect-like bias in healthy volunteers with the interleaved TMS/fMRI technique: preliminary evidence. Front. Hum. Neurosci. 6 Available at https://www.frontiersin.org/articles/10.3389/fnhum.2012.00326/full. [Accessed April 3, 2020].
Sack, AT, Kohler, A, Bestmann, S, Linden, DEJ, Dechent, P, Goebel, R, Baudewig, J, 2007. Imaging the brain activity changes underlying impaired visuospatial judgments: simultaneous fMRI, TMS, and behavioral studies. Cereb. Cortex 17, 2841–2852.
Schenkenberg, T, Bradford, DC, Ajax, ET, 1980. Line bisection and unilateral visual neglect in patients with neurologic impairment. Neurology 30, 509–517.

Schintu, S, Chaumillon, R, Guillaume, A, Salemme, R, Reilly, KT, Pisella, L, Farnè, A, 2020a. Eye dominance modulates visuospatial attention. Neuropsychologia 141, 107314.
Schintu, S, Freedberg, M, Gotts, SJ, Cunningham, CA, Alam, ZM, Shomstein, S, Wassermann, EM, 2020b. Prism adaptation modulates connectivity of the intraparietal sulcus with multiple brain networks. Cereb Cortex 30, 4747–4758.
Schintu, S, Patané, I, Caldano, M, Salemme, R, Reilly, KT, Pisella, L, Farnè, A, 2017. The asymmetrical effect of leftward and rightward prisms on intact visuospatial cognition. Cortex 97, 23–31.
Schintu, S, Pisella, L, Jacobs, S, Salemme, R, Reilly, KT, Farnè, A, 2014. Prism adaptation in the healthy brain: the shift in line bisection judgments is long lasting and fluctuates. Neuropsychologia 53, 165–170.
Seydell-Greenwald, A, Pu, SF, Ferrara, K, Chambers, CE, Newport, EL, Landau, B, 2019. Revisiting the Landmark Task as a tool for studying hemispheric specialization: what's really right? Neuropsychologia 127, 57–65.
Shah-Basak, PP, Chen, P, Caulfield, K, Medina, J, Hamilton, RH, 2018. The role of the right superior temporal gyrus in stimulus-centered spatial processing. Neuropsychologia 113, 6–13.
Shulman, GL, Pope, DLW, Astafiev, SV, McAvoy, MP, Snyder, AZ, Corbetta, M, 2010. Right hemisphere dominance during spatial selective attention and target detection occurs outside the dorsal frontoparietal network. J. Neurosci. Off J. Soc. Neurosci. 30, 3640–3651.
Siebner, HR, Peller, M, Willoch, F, Auer, C, Bartenstein, P, Drzezga, A, Schwaiger, M, Conrad, B, 1999. Imaging functional activation of the auditory cortex during focal repetitive transcranial magnetic stimulation of the primary motor cortex in normal subjects. Neurosci. Lett. 270, 37–40.
Szczepanski, SM, Kastner, S, 2013. Shifting attentional priorities: control of spatial attention through hemispheric competition. J. Neurosci. 33, 5411–5421.
Talairach, J, Tournoux, P, 1988. Co-Planar Stereotaxic Atlas of the Human Brain, 2. Thieme Medical Publishers, N Y.
Taylor, PA, Saad, ZS, 2013. FATCAT: (an efficient) functional and tractographic connectivity analysis toolbox. Brain Connect 3, 523–535.
Thiebaut de Schotten, M, Dell'Acqua, F, Forkel, SJ, Simmons, A, Vergani, F, Murphy, DGM, Catani, M, 2011. A lateralized brain network for visuospatial attention. Nat. Neurosci. 14, 1245–1246.
Tzourio, N, El Massioui, F, Crivello, F, Joliot, M, Renault, B, Mazoyer, B, 1997. Functional anatomy of human auditory attention studied with PET. Neuroimage 5, 63–77.
Valero-Cabré, A, Toba, MN, Hilgetag, CC, Rushmore, RJ, 2020. Perturbation-driven paradoxical facilitation of visuo-spatial function: revisiting the 'sprague effect.'. Cortex 122, 10–39.
Vallar, G, 1998. Spatial hemineglect in humans. Trends Cogn. Sci. 2, 87–97.
Vallar, G, Perani, D, 1986. The anatomy of unilateral neglect after right-hemisphere stroke lesions. A clinical/CT-scan correlation study in man. Neuropsychologia 24, 609–622.
Vercauteren, K, Pleysier, T, Van Belle, L, Swinnen, SP, Wenderoth, N, 2008. Unimanual muscle activation increases interhemispheric inhibition from the active to the resting hemisphere. Neurosci. Lett. 445, 209–213.
Verdon, V, Schwartz, S, Lovblad, K-O, Hauert, C-A, Vuilleumier, P, 2010. Neuroanatomy of hemispatial neglect and its functional components: a study using voxel-based lesion-symptom mapping. Brain 133, 880–894.
Wang, L, Mruczek, REB, Arcaro, MJ, Kastner, S, 2015. Probabilistic maps of visual topography in human cortex. Cereb Cortex N Y NY 25, 3911–3931.
Weissgerber, TL, Milic, NM, Winham, SJ, Garovic, VD, 2015. Beyond bar and line graphs: time for a new data presentation paradigm. PLoS Biol. 13, e1002128.
World Medical Association, 2013. World medical association declaration of helsinki: ethical principles for medical research involving human subjects. JAMA 310, 2191–2194.